Genome-Wide Scan for Japanese Familial Intracranial Aneurysms

Linkage to Several Chromosomal Regions

Shigeki Yamada, MD*; Maki Utsunomiya, MPH*; Kayoko Inoue, MD, MPH; Kazuhiko Nozaki, MD, PhD; Sumiko Inoue, PhD; Katsunobu Takenaka, MD, PhD; Nobuo Hashimoto, MD, PhD; Akio Koizumi, MD, PhD

Background—Genetic factors have an important role in the pathogenesis of intracranial aneurysm (IA). The results of previous studies have suggested several loci.

Methods and Results—From 29 IA families with ≥3 individuals affected by IA, we used nonparametric (model-free) methods for linkage analyses, using GENEHUNTER and Merlin software. Genome-wide linkage analyses revealed 3 regions on chromosomes 17cen (maximum nonparametric logarithm of the odds score [MNS] = 3.00, nominal P=0.001), 19q13 (MNS=2.15, nominal P=0.020), and Xp22 (MNS=2.16, nominal P=0.019). We tested 4 candidate genes in these regions: the microfibril-associated protein 4 gene (*MFAP4*) and the promoter polymorphism of the inducible nitric oxide synthase gene (*NOS2A*) on chromosome 17cen, the epsilon genotypes of the apolipoprotein E gene (*APOE*) on chromosome 19q13, and the angiotensin I converting enzyme 2 gene (*ACE2*) on chromosome Xp22. Associations of their polymorphisms with IA were evaluated by a case-control study (100 cases: 29 probands from IA families and 71 unrelated subjects with IAs, 100 unrelated control subjects [unaffected members with IAs and absence of family history of IAs]). However, the case-control study showed that none of the polymorphisms of the examined genes had associations with IA.

Conclusions—A genome-wide scan in 29 Japanese families with a high degree of familial clustering revealed 1 suggestive linkage region on chromosome 17cen and 2 potentially interesting regions on chromosomes 19q13 and Xp22. These regions were consistent with previous findings in various populations. (***Circulation.*** **2004;110:3727-3733.)**

Key Words: aneurysm ■ cerebrovascular disorders ■ genes ■ stroke

Family members of patients with subarachnoid hemorrhage (SAH) have been documented to have a high risk of SAH and a high prevalence of unruptured intracranial aneurysms (IAs).[1,2] The risk of ruptured IAs in first-degree relatives of patients with aneurysmal SAH is ≈4 times higher than that in the general population.[2] Genetic and environmental factors play important roles in the pathogenesis of IA, and recent progress in molecular genetics enables the genetic determinants to be approached directly.

Genome-wide linkage analyses for familial IA have been reported by 2 groups.[3,4] Onda et al[3] suggested linkage to regions on chromosomes 5q22–31 (maximum LOD score [MLS] 2.24), 7q11 (MLS 3.22), and 14q22 (MLS 2.31) in 104 Japanese affected sibling pairs. The linkage to 7q11 was replicated by another study in a white population,[5] although we could not confirm the linkage to this locus in Japanese.[6] Olson et al[4] found suggestive linkages on chromosomes 19q12–13 (MLS 2.58) and Xp22 (MLS 2.08) in 48 Finnish affected sibling pairs, a linkage confirmed by another study.[7] These results suggest that multiple genes determine susceptibility to IA.

In the present study, we conducted a family-based approach because high degrees of familial clustering of IAs can raise relative risks and thereby provide us a better chance to isolate the major locus.[8] We recruited 29 families with ≥3 affected members and report here the results of genome-wide linkage analysis.

Methods

Families

From collaborating hospitals in the western part of Japan, we recruited patients with IA who had a family history of IAs or SAH.

Received May 20, 2004; revision received July 15, 2004; accepted August 2, 2004.

From the Department of Health and Environmental Sciences (S.Y., M.U., K.I., S.I., A.K.) and the Department of Neurosurgery (S.Y., K.N., N.H.), Kyoto University Graduate School of Medicine, Kyoto, Japan; and the Department of Neurosurgery, Takayama Red Cross Hospital (K.T.), Gifu, Japan.

*Drs Yamada and Utsunomiya contributed equally to this work.

The online-only Data Supplement, which contains Tables I through III, is available with this article at http://www.circulationaha.org.

Correspondence to Dr Akio Koizumi, Department of Health and Environmental Sciences, Graduate School of Medicine Kyoto University, Konoe-cho, Yoshida, Sakyo-ku, Kyoto, 606-8501, Japan. E-mail koizumi@pbh.med.kyoto-u.ac.jp

Circulation **is available at http://www.circulationaha.org** **DOI: 10.1161/01.CIR.0000143077.23367.18**

If they had ≥3 family members with IAs or SAH and ≥2 including the proband were alive, their families were regarded as suitable subjects for the present study. "Affected" status of participants was determined in 2 ways. First, if participants had been diagnosed with IAs or SAH, they were confirmed as having saccular IAs from their medical records. Second, if participants aged ≥30 years did not know whether they had had IAs, they underwent magnetic resonance angiography (MRA) for screening of IAs. All MRA images were examined by ≥3 neurosurgeons or neuroradiologists. If IAs were suspected by MRA, additional examinations, such as digital subtraction angiography and 3-dimensional computed tomography, were conducted. Families with known heritable diseases associated with IAs, such as Ehlers-Danlos syndrome type IV, Marfan syndrome, neurofibromatosis type 1, or autosomal dominant polycystic kidney disease, were excluded from this study.[9,10] Details of the methods of participation and data collection have been reported previously.[6] The methods used in this study conformed to the tenets of the Declaration of Helsinki and received approval from the Ethics Committee of Kyoto University.

Genotyping

Genomic DNA was extracted from blood samples (in 2 cases, from a preserved umbilical cord) with a QIAamp DNA Blood Mini Kit (Qiagen Inc). Polymerase chain reaction (PCR) amplification from genomic DNA was performed with fluorescence-labeled (6-FAM, HEX, NED) and tailed primers. PCR primers to analyze microsatellite markers comprised an ≈10-cM human index map (ABI Prism Linkage Mapping Set Version 2: 382 markers for 22 autosomes and 18 markers for the X chromosome), and other microsatellite fine markers were designed according to information from the UniSTS map.[11] PCR reactions were carried out in 7.5 μL with 50 ng genomic DNA, using AmpliTaq Gold DNA Polymerase (Applied Biosystems) in a 2-step amplification program. DNA fragments were analyzed on an ABI Prism 3100 Avant Genetic Analyzer. Genotyping errors and inconsistent relationships were checked with the use of SimWalk2 and Merlin software.[12,13] If the results of genotyping were missed or ambiguous, we treated them as an unknown genotype for the linkage analysis.

Linkage Analysis

Unaffected members who were ≥60 years of age and underwent MRA screening and affected members were included for the linkage analysis. The inheritance patterns of familial IA have not been determined, though autosomal dominant, recessive, and undetermined modes have been reported in familial IA[9,14]; we thus used only a nonparametric method. In addition, the phenotype of unaffected members was assigned as "unknown" in this study. The purpose of including unaffected members was to increase the accuracy of haplotype estimation in affected members, although inclusion did not increase the statistical power. Multipoint nonparametric analyses for autosomes and X chromosome were run with 1-tailed probability values (P), using GENEHUNTER (Version 2.0 and 1.3) and Merlin software.[13,15] Population allele frequencies for each microsatellite marker were estimated from the founders of IA families. We used a 2-stage design: First, all chromosomal regions were screened by genotyping at an ≈10-cM density (screening), and the region, of which nominal $P<0.05$ of the nonparametric logarithm of the odds (NPL) score, was considered as a potentially interesting region. Second, these regions were further finely mapped at ≈1- to 2-cM densities (fine mapping). Nominal $P<0.05$ regions were again considered as potentially interesting regions or nominal $P<0.001$ regions were considered as suggestive linkage regions.[15]

We evaluated statistical power through the use of simulations, as previously reported.[6] Simulations were run 1000 times by GENEHUNTER to obtain a false-negative rate (ie, sensitivity, percentage) when the threshold of nominal P was equal to 0.05 under conditions of 75%, 50%, and 25% of locus heterogeneities among families for the linkage analysis.

Case-Control Study

To test associations of polymorphisms of candidate genes (described below) in suggestive linkage or potentially interesting regions with IA, we conducted a case-control study. In the case-control study, 100 cases and 100 control subjects were enrolled from collaborating hospitals in western Japan. Control subjects had the following characteristics: (1) confirmation of not harboring IA by digital subtraction angiography, 3-dimensional computed tomography, or MRA, (2) age at the time of diagnosis ≥40 years, (3) no medical history of any stroke including IAs or SAH, and (4) no family history of IAs or SAH in first-degree relatives. Cases were composed of unrelated subjects whose presence of IA had been confirmed by angiography or operation and family probands.

The allele frequencies of candidate genes in cases and control subjects were compared by the contingency table of $\chi 2$ test statistics, with the use of SAS software (Version 8.2, SAS Institute Inc).

Candidate Genes

To search for mutations or polymorphisms of the microfibril-associated protein 4 gene (*MFAP4*, GenBank accession number = NT_030843) and the angiotensin I converting enzyme (*ACE*) 2 gene (ACE2, NT_011757), genomic DNA from the probands was used as a template to generate PCR products, which then were sequenced directly. Forward and reverse PCR primers for each coding exon were selected in an intronic sequence ≥50 bp away from the intron/exon boundaries (Data Supplement Table I). PCR products were run on 2% agarose gel, and the appropriate bands were excised and then purified with the use of the QIAquick Gel Extraction Kit (Qiagen). PCR and sequencing primers are shown in Data Supplement Table I. Sequencing results were analyzed on an ABI Prism 3100 Avant DNA sequencer (Applied Biosystems). Any polymorphic sites identified through our sequencing were searched for registered single nucleotide polymorphisms (SNPs) at the web site of the National Center for Biotechnology Information database SNP (dbSNP).[16]

Restriction enzymes to determinate the genotypes of found polymorphisms were *BbvCI* for the *MFAP4*, *AluI* for the *ACE2*, and *HhaI* for the apolipoprotein E (*APOE*, *NT*_011109),[17] respectively. The bi-allelic AAAT-repeat located 2.45 kbp upstream from the start codon of the inducible nitric oxide synthase (iNOS) gene (*NOS2A*, NT_010799) was determined by the length of the PCR products amplified by using primers designed according to a DNA sequence found from GenBank (D29675).[18]

Results

Characterization of Families

Twenty-nine families met our criteria (≥3 affected members in a family) and were enrolled in this study (Figure 1). In the 29 families, 116 asymptomatic family members (59 men, 57 women, 30 to 82 years of age; mean, 50.0 years) without a history of IAs or SAH underwent MRA examinations. Of the 116 examinees, 22 (8 men [13.6%] and 14 women [24.6%]) were found to have IAs. Of a total 105 affected members (35 men, 70 women) in the 29 families, 70 affected members (66.7%) had SAH and 35 affected members (33.3%) have or have had unruptured IAs. The mean age at the time of diagnosis with SAH among the 70 affected members was 55.4 years (51.7 among 23 men, 57.3 among 47 women). Eighteen affected members had died of SAH.

Linkage Analysis

Eighty-seven living affected members were genotyped through blood DNA; 2 affected members who had died (IV-1 in Pedigree 5 and III-10 in Pedigree 29) were genotyped through DNA from their preserved umbilical cords. Genotypes of 4 deceased affected members (II-4 in Pedigree 1, II-5

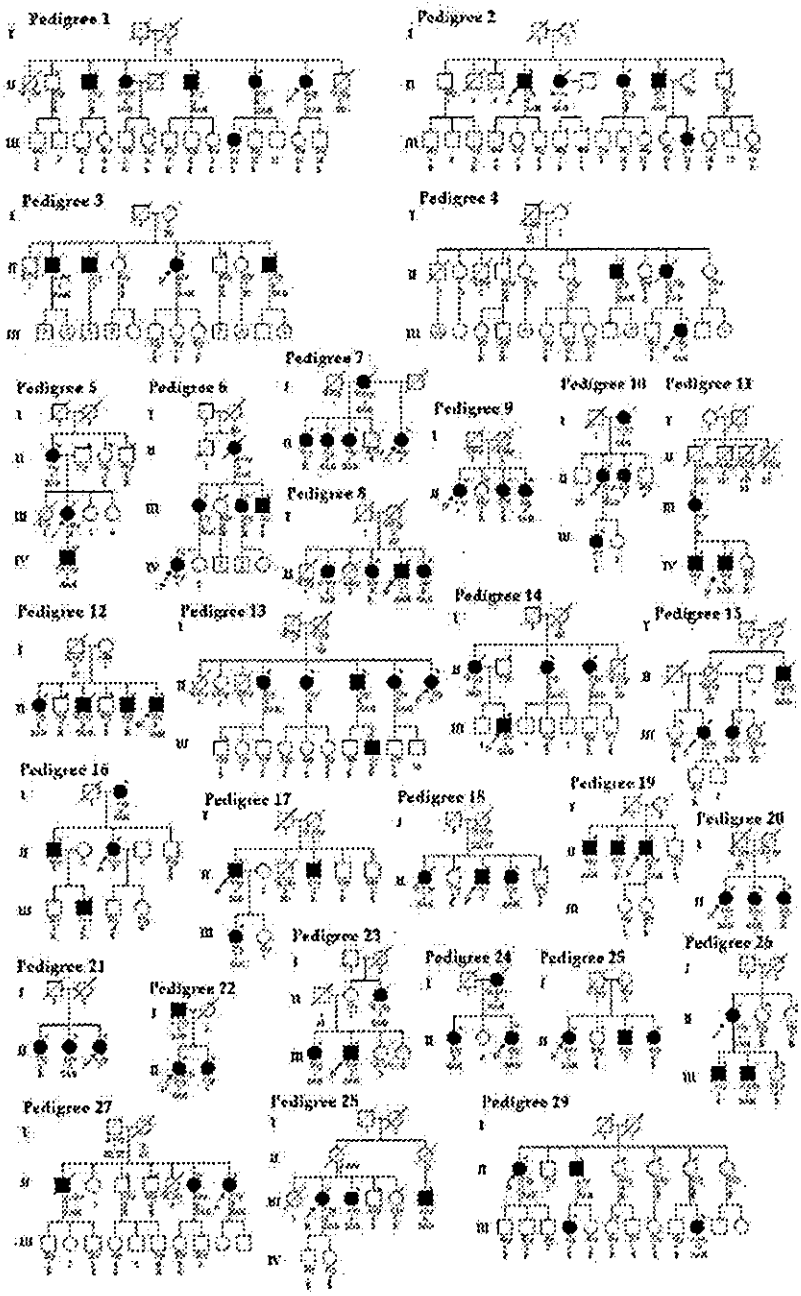

Figure 1. Twenty-nine families in genetic linkage analysis. □, Male; ○, female; ■, affected members (IA or SAH); ●, individual died. *Participation in linkage analysis: P, proband; SAH, subarachnoid hemorrhage; ST, stroke; SD, sudden death by unknown cause; E, examination with MRA; and d, age at death.

in Pedigree 2, II-1 in Pedigree 14, and II-1 in Pedigree 27) were reconstructed from the genotypes of offspring and spouses. In total, 93 affected members (31 men, 62 women; mean age at diagnosis, 55.2 years) and 27 unaffected members (13 males, 14 females, aged ≥60 years) were included in the linkage analysis. Characteristics of these members are shown in Table 1. The genome-wide linkage results in the screening are shown in Figure 2. Regions of potentially interest (nominal $P<0.05$) by multipoint NPL scores were observed on chromosomes 12q11–13, 15q21, 17cen, 19q13, and Xp22 (Table 2 and Data Supplement Table II).

The statistical power of this screening was 52%, 93%, and 99% when the locus heterogeneity was 75%, 50%, and 25%, respectively.

After fine mapping, 2 of 5 regions, 19q13 (maximum NPL score [MNS] = 2.15, nominal $P=0.020$) and Xp22 (MNS=2.16, nominal $P=0.019$), remained potentially interesting regions (Table 2 and Data Supplement Table III). The region on chromosome 17cen turned out to be a suggestive linkage region (MNS=3.00, nominal $P=0.001$). The sizes of regions with nominal $P<0.05$ were 17.7 cM (D17S921–D17S1800) on chromosome 17, 7.9 cM (D19S198–

TABLE 1. Characteristics of Family Members in the Linkage Analysis

	Affected			Unaffected		
	Male (n=31)	Female (n=62)	Total (n=93)	Male (n=13)	Female (n=14)	Total (n=27)
Age at diagnosis, y, mean±SD	53.6±13.8	56.0±11.7	55.2±12.4	66.2±3.9	67.1±7.2	66.7±5.7
Hypertension, %	36.7	44.3	40.9	38.5	35.7	37.0
Current or ex-smoker, %	70.0	29.5	41.9	76.9	7.1	40.7
Subarachnoid hemorrhage, %	61.3	62.9	62.4	...	...	...
Multiple IAs, %	12.9	19.4	17.2	...	...	...

Those classified as "Affected" were diagnosed as harboring IAs. Those classified as "Unaffected" were diagnosed as free from IAs by MRA and were ≥60 y of age.

D19S596) on chromosome 19, and 10.1 cM (DXS987–DXS7593) on chromosome X. Physical localization of microsatellite markers in these regions and candidate genes are shown in Table 3.

Case-Control Study for Candidate Genes

We searched putative candidate genes in 1 suggestive linkage and 2 potentially interesting regions after considering physiological functions and documented evidence: chromosomes

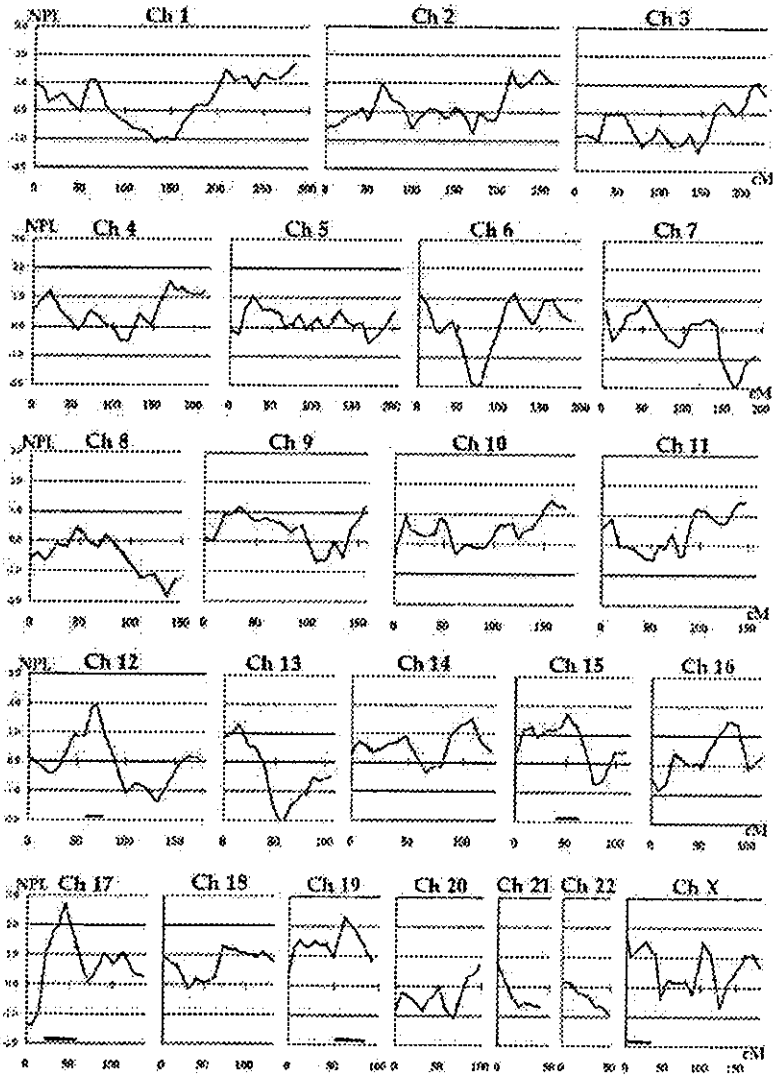

Figure 2. Multipoint nonparametric logarithm of odds score in genome-wide screening. Bars at bottom of chart indicate regions genotyped further in fine mapping.

TABLE 2. Maximum Multipoint NPL Scores

	Screening		Fine Mapping	
Region	NPL Score	Nominal *P*	NPL Score	Nominal *P*
12q11–13	1.96	0.032	1.15	0.126
15q21	1.71	0.043	0.80	0.209
17cen	2.74	0.003	3.00	0.001
19q13	2.33	0.014	2.15	0.020
Xp22	1.80	0.040	2.16	0.019

Regions were those exceeding the threshold (nominal $P<0.05$) of the NPL score in the screening. Screening was genotyping all chromosomal regions at ~10-cM density. Fine mapping was genotyping at ~1- to 2-cM densities.

17cen (*NOS2A* and *MFAP4*), 19q13 (*APOE*), and Xp22 (*ACE2*) (Table 3). In *NOS2A*, there was the 4-bp (AAAT) deletion (R4)/insertion (R5) polymorphism in the regulatory region, and R5 was a high-risk allele of hypertension and coronary artery stenosis.[18–20] We therefore tested the association of this polymorphism. Characteristics of the case versus control subjects are shown in Table 4. All cases and control subjects had an R4/R4 genotype (100%) (Table 5).

We next checked whether the epsilon (ϵ) genotypes of *APOE* were involved in IA because the *APOE* ϵ-4 genotype has been reported as a risk factor for SAH among Japanese.[21] The relevant allele frequencies in 100 cases were $\epsilon-2=4\%$, $\epsilon-3=85\%$, and $\epsilon-4=11\%$, which were not different from 100 control subjects (Table 5) and the Japanese general population.[22] Six genotype frequencies were $\epsilon-2/\epsilon-2=0\%$, $\epsilon-2/\epsilon-3=7.0\%$, $\epsilon-2/\epsilon-4=0.5\%$, $\epsilon-3/\epsilon-3=69.9\%$, $\epsilon-3/\epsilon-4=20.6\%$, and $\epsilon-4/\epsilon-4=2.0\%$ in cases, being the same in control subjects. These did not differ significantly from those expected from the Hardy-Weinberg equilibrium. Furthermore, there was no family in which the $\epsilon-4$ allele of *APOE* was segregated with IA (data not shown).

TABLE 3. Physical Localization of Microsatellite Markers and Candidate Genes

Ch	Position, kb	Marker/Gene	NPL	Nominal *P*
17	14461	D17S921	1.42	0.080
17	15356	D17S918	2.50	0.006
17	16616	D17S1857	2.88	0.002
17	17465	D17S2196	3.00	0.001
17	**19450**	*MFAP4*		
17	19731	AFMa126yd5	2.78	0.003
17	20924	D17S1871	2.40	0.008
17	21493	D17S783	1.95	0.030
17	**26250**	*NOS2A*		
17	26806	D17S1824	1.95	0.030
17	28528	D17S1294	1.94	0.030
17	30082	D17S1800	1.41	0.080
19	46845	D19S198	0.96	0.200
19	48501	D19S420	1.73	0.040
19	49815	D19S574	1.83	0.030
19	**50100**	*APOE*		
19	51703	D19S412	2.15	0.020
19	52665	D19S596	1.56	0.060
X	14071	DXS987	1.33	0.090
X	**14960**	*ACE2*		
X	17103	DXS8019	2.16	0.020
X	21755	DXS7593	1.61	0.050

Positions should be referred to human genome sequence information at the National Center for Biotechnology Information web site (http://www.ncbi.nlm.nih.gov/genome/guide/human/).

TABLE 4. Characteristics of Cases vs Controls

	Cases*	Controls†
No. (male/female)	100 (34/66)	100 (39/61)
Age at diagnosis, y		
Mean±SD	58.7±9.4	58.4±10.1
Range	38–78	40–83
Family history of IA, %	50	0
Hypertension, %	45	26
Current or ex-smoker, %	40	26

*Cases were 29 family probands and 71 unrelated subjects confirmed with IAs by operation or digital subtraction angiography.

†Controls were diagnosed as without IAs by digital subtraction angiography or MRA.

We sequenced entire coding regions of *MFAP4* and *ACE2* in the 29 probands of the IA families (Data Supplement Table I). However, we found no polymorphism in the coding regions of these genes. One novel SNP was identified in intron 4 of *MFAP4*, of which the allele frequency (G/A) was essentially the same between 200 case and 200 control chromosomes (Table 5). One registered SNP (dbSNP: rs2285666) was identified in intron 3 of *ACE2*, in which allele frequency (C/T) did not differ between 200 case and 200 control chromosomes (Table 5).

Discussion

Linkage Analysis

We found 1 suggestive linkage region on chromosome 17cen and 2 potentially interesting (nominal $P<0.05$) regions on chromosomes 19q13 and Xp22. The suggestive linkage region on chromosome 17cen was in accord with the results of a previous Japanese sib-pair analysis (nominal $P=0.027$),[3] whereas 2 potentially interesting regions on chromosomes 19q13 and Xp22 were reported as candidate regions in a Finish population.[4] The region on chromosome 19q13 was also replicated by another Finish study.[7] The region on chromosome 19q13 may thus not be specific to Finnish population. Collectively, candidate regions that have to date been replicated in >1 study include 7q11 (Onda et al and Farnham et al) and 19q13 (Olson et al and Van Der Voet et al).[3–5,7] The regions of 17cen (Onda et al[3]) and Xp22 (Olson et al[4]) are extended in the present study. Such concordant regions should be considered as high-priority loci and provide promising scaffolds for future studies to identify the exact genetic mechanisms for IA. On the other hand, scattering over various chromosomes may suggest some complexity to the pathophysiology of IAs; such complexity represents the

TABLE 5. Case-Control Study for Candidate Genes

Gene	Base Position*	Location	Allele	Allele Frequency,† n		χ^2	*P*
				Cases	Controls		
MFAP4	+1824	Intron 4	G	193	188	1.38	0.240
			A	7	12		
NOS2A	−2453	Promoter	$(AAAT)_4$	200	200	...	...
			$(AAAT)_5$	0	0		
APOE	+2059, +2197	Exon 4	ϵ−2	8	7	1.493	0.474
			ϵ−3	171	164		
			ϵ−4	21	29		
ACE2	+8686	Intron 3	C	75	80	0.666	0.414
			T	91	81		

*The number from the A of the start codon (ATG) in the genomic DNA reference sequence.
†Allele frequency was described chromosome number.

complexity of interactions among many genetic and environmental risk factors that contribute in different degrees with different populations.

It is well known that female sex is a risk factor for IA. The reasons for this increased prevalence are unknown, but there could be a genetic basis as demonstrated in this study. It has recently been shown that many genes ("escapees") on chromosome Xp22 escape inactivation,[23] which may explain the sex differences in susceptibility to IA by gene dosage effects.

The present study has several limitations. First, because we took a family-based approach, it was hard to narrow down the candidate regions to 1-cM resolution. These candidate regions still have ≈8- to 18-cM sizes, and further efforts will be needed to find susceptibility genes for IA. For this goal, linkage disequilibrium (LD) mapping will be required. The second limitation is associated with the statistical power and specificity. Although the statistical power is highly dependent on the locus heterogeneity, it is hard to predict what degrees of locus heterogeneity exist among the 29 families. Simulation could, however, provide a prediction of the statistical power; >90% power was obtainable if the locus heterogeneity was <50%.

Candidate Genes

At least 2 mechanisms are hypothesized to play critical roles in the development of IA. These include defects in the maintenance of extracellular matrix and in remodeling. These hypotheses suggest *MFAP4* and *iNOS* on chromosome 17cen[9,10,24–26] and *ACE2* on chromosome X p22[27–29] as candidate genes. On the other hand, an epidemiological study among Japanese ranked *APOE* high as a candidate gene on chromosome 19q13.[21] However, in the case-control study, albeit with very limited numbers of plausible genes, candidate genes including *APOE* failed to show positive associations with IA. Obviously, LD mapping covering entire regions is required to search for clues to susceptibility genes.

Conclusions

Linkage analyses in 29 IA families with ≥3 affected members showed 1 suggestive linkage region on chromosome 17cen (17.7 cM) and potentially interesting regions on chromosomes 19q13 (7.9 cM) and Xp22 (10.1 cM). These 3 loci provide promising scaffolds for searching for genes determining susceptibility to IA. We also showed evidence that 4 candidate genes, *MFAP4*, *ACE2*, a promoter variant of *NOS2A*, and *APOE* ϵ genotypes, did not have LD with an unknown susceptibility gene for IA. Further efforts are clearly needed to identify susceptibility genes for IA.

Acknowledgments

This work was supported by a grant from the Ministry of Education, Science, Sports, and Culture of Japan (Kiban Kenkyuu A: 14207016) and a grant from the Japan Society for the Promotion of Science (15012231). We are grateful to Dr Mark G. Lathrop (The Centre National de Genotypage, Evry, France) for critical reading of the manuscript. We thank Miho Yoshida and Norio Matsuura for technical assistance and the following doctors for patient recruitment and help in ascertaining MRA examinations: Susumu Miyamoto (National Cardiovascular Center), Shiro Nagasawa and Nobuhisa Mabuchi (Soseikai General Hospital), Yasuhiko Tokuriki and Tomoo Tokime (Fukui Red Cross Hospital), Takaaki Kaneko and Nozomu Murai (Hikone Municipal Hospital), Shunichi Yoneda and Yoshito Naruo (Nihonbashi Hospital), Sen Yamagata (Kurashiki Central Hospital), Kenji Hashimoto (Hyogo Prefectural Tsukaguchi Hospital), Atsushi Okumura and Yoshihiko Uemura (Kyoto City Hospital), Tomohiko Iwai (Gifu Municipal Hospital), Hiroyasu Yamakawa (Geroonsen Hospital), Shingo Sugimoto (Sumi Hospital), Atsushi Kawarazaki (Kawarazaki Hospital), Kiyohiro Houkin and Osamu Houmou (Sapporo Medical University School of Medicine), Akira Ogawa and Miyuki Abe (Iwate Medical University), Masayuki Matsuda (Shiga University of Medical Science), Michiyasu Suzuki and Sadahiro Nomura (Yamaguchi University School of Medicine), Izumi Nagata (Nagasaki University School of Medicine), Masatsune Ishikawa (Kitano Hospital), Shinichiro Okamoto (Osaka Red Cross Hospital), Yoshinori Akiyama (Tenri Hospital), Takeshi Nishihara (Kouseikai Takeda Hospital), Hiroshi Kajikawa and Shinichi Wakabayashi (Kajikawa Hospital), Akihiro Doi and Junji Yoshioka (Okayama Kyokuto Hospital), Kazunori Kajihara and Yuji Okamoto (Saiseikai Yahata Hospital), Ichiro Nakahara and Toshio Higashi (Kokura Memorial Hospital), and Takashi Yoshizawa and Kenjiro Ito (Yokohama Shintoshi Neurosurgical Hospital).

References

1. Okamoto K, Horisawa R, Kawamura T, Asai A, Ogino M, Takagi T, Ohno Y. Family history and risk of subarachnoid hemorrhage: a case-control study in Nagoya, Japan. *Stroke*. 2003;34:422–426.

2. Ronkainen A, Miettinen H, Karkola K, Papinaho S, Vanninen R, Puranen M, Hernesniemi J. Risk of harboring an unruptured intracranial aneurysm. *Stroke*. 1998;29:359–362.
3. Onda H, Kasuya H, Yoneyama T, Takakura K, Hori T, Takeda J, Nakajima T, Inoue I. Genome-wide linkage and haplotype-association studies map intracranial aneurysm to chromosome 7q11. *Am J Hum Genet*. 2001;69:804–819.
4. Olson JM, Vongpunsawad S, Kuivaniemi H, Ronkainen A, Hernesniemi J, Ryynanen M, Kim LL, Tromp G. Search for intracranial aneurysm susceptibility gene(s) using Finnish families. *BMC Med Genet*. 2002;3:7.
5. Farnham JM, Camp NJ, Neuhausen SL, Tsunoda J, Parker D, MacDonald J, Cannon-Albright LA. Confirmation of chromosome 7q11 locus for predisposition to intracranial aneurysm. *Hum Genet*. 2004;114:250–255.
6. Yamada S, Utsunomiya M, Inoue K, Nozaki K, Miyamoto S, Hashimoto N, Takenaka K, Yoshinaga T, Koizumi A. Absence of linkage of familial intracranial aneurysms to 7q11 in highly aggregated Japanese families. *Stroke*. 2003;34:892–900.
7. Van Der Voet M, Olson JM, Kuivaniemi H, Dudek DM, Skunca M, Ronkainen A, Niemela M, Jaaskelainen J, Hernesniemi J, Helin K, Leinonen E, Biswas M, Tromp G. Intracranial aneurysms in Finnish families: confirmation of linkage and refinement of the interval to chromosome 19q13.3. *Am J Hum Genet*. 2004;74:564–571.
8. Lander ES, Schork NJ. Genetic dissection of complex traits. *Science*. 1994;265:2037–2048.
9. Schievink WI. Genetics of intracranial aneurysms. *Neurosurgery*. 1997; 40:651–663.
10. Schievink WI, Parisi JE, Piepgras DG, Michels VV. Intracranial aneurysms in Marfan's syndrome: an autopsy study. *Neurosurgery*. 1997;41: 866–871.
11. National Center for Biotechnology Information. Summary of Maps in UniSTS. Available at: http://www.ncbi.nlm.nih.gov/genome/sts/. Accessed March 1, 2004.
12. Sobel E, Papp JC, Lange K. Detection and integration of genotyping errors in statistical genetics. *Am J Hum Genet*. 2002;70:496–508.
13. Abecasis GR, Cherny SS, Cookson WO, Cardon LR. Merlin: rapid analysis of dense genetic maps using sparse gene flow trees. *Nat Genet*. 2002;30:97–101.
14. Wills S, Ronkainen A, van der Voet M, Kuivaniemi H, Helin K, Leinonen E, Frosen J, Niemela M, Jaaskelainen J, Hernesniemi J, Tromp G. Familial intracranial aneurysms: an analysis of 346 multiplex Finnish families. *Stroke*. 2003;34:1370–1374.
15. Kruglyak L, Daly MJ, Reeve-Daly MP, Lander ES. Parametric and nonparametric linkage analysis: a unified multipoint approach. *Am J Hum Genet*. 1996;58:1347–1363.
16. National Center for Biotechnology Information. Single Nucleotide Polymorphism. Available at: http://www.ncbi.nlm.nih.gov/SNP/. Accessed March 1, 2004.
17. Hixson JE, Vernier DT. Restriction isotyping of human apolipoprotein E by gene amplification and cleavage with HhaI. *J Lipid Res*. 1990;31: 545–548.
18. Kunnas TA, Mikkelsson J, Ilveskoski E, Tanner MM, Laippala P, Penttila A, Perola M, Nikkari ST, Karhunen PJ. A functional variant of the iNOS gene flanking region is associated with LAD coronary artery disease: an autopsy study. *Eur J Clin Invest*. 2003;33:1032–1037.
19. Glenn CL, Wang WY, Morris BJ. Different frequencies of inducible nitric oxide synthase genotypes in older hypertensives. *Hypertension*. 1999;33: 927–932.
20. Morris BJ, Glenn CL, Wilcken DE, Wang XL. Influence of an inducible nitric oxide synthase promoter variant on clinical variables in patients with coronary artery disease. *Clin Sci (Lond)*. 2001;100:551–556.
21. Kokubo Y, Chowdhury AH, Date C, Yokoyama T, Sobue H, Tanaka H. Age-dependent association of apolipoprotein E genotypes with stroke subtypes in a Japanese rural population. *Stroke*. 2000;31:1299–1306.
22. Zaman MM, Ikemoto S, Yoshiike N, Date C, Yokoyama T, Tanaka H. Association of apolipoprotein genetic polymorphisms with plasma cholesterol in a Japanese rural population: the Shibata Study. *Arterioscler Thromb Vasc Biol*. 1997;17:3495–3504.
23. Carrel L, Cottle AA, Goglin KC, Willard HF. A first-generation X-inactivation profile of the human X chromosome. *Proc Natl Acad Sci U S A*. 1999;96:14440–14444.
24. Fukuda S, Hashimoto N, Naritomi H, Nagata I, Nozaki K, Kondo S, Kurino M, Kikuchi H. Prevention of rat cerebral aneurysm formation by inhibition of nitric oxide synthase. *Circulation*. 2000;101:2532–2538.
25. Iwashina M, Shichiri M, Marumo F, Hirata Y. Transfection of inducible nitric oxide synthase gene causes apoptosis in vascular smooth muscle cells. *Circulation*. 1998;98:1212–1218.
26. Sadamasa N, Nozaki K, Hashimoto N. Disruption of gene for inducible nitric oxide synthase reduces progression of cerebral aneurysms. *Stroke*. 2003;34:2980–2984.
27. Ohkuma H, Suzuki S, Fujita S, Nakamura W. Role of a decreased expression of the local renin-angiotensin system in the etiology of cerebral aneurysms. *Circulation*. 2003;108:785–787.
28. Slowik A, Borratynska A, Pera J, Betlej M, Dziedzic T, Krzyszkowski T, Czepko R, Figlewicz DA, Szczudlik A. II genotype of the angiotensin-converting enzyme gene increases the risk for subarachnoid hemorrhage from ruptured aneurysm. *Stroke*. 2004;35:1594–1597.
29. Takenaka K, Yamakawa H, Sakai H, Yoshimura S, Murase S, Okumura A, Nakatani K, Kimura T, Nishimura Y, Yoshimi N, Sakai N. Angiotensin I-converting enzyme gene polymorphism in intracranial saccular aneurysm individuals. *Neurol Res*. 1998;20:607–611.

Magnitude and Role of Wall Shear Stress on Cerebral Aneurysm

Computational Fluid Dynamic Study of 20 Middle Cerebral Artery Aneurysms

Masaaki Shojima, MD; Marie Oshima, PhD; Kiyoshi Takagi, MD, PhD; Ryo Torii, PhD; Motoharu Hayakawa, MD, PhD; Kazuhiro Katada, MD, PhD; Akio Morita, MD, PhD; Takaaki Kirino, MD, PhD

Background and Purpose—Wall shear stress (WSS) is one of the main pathogenic factors in the development of saccular cerebral aneurysms. The magnitude and distribution of the WSS in and around human middle cerebral artery (MCA) aneurysms were analyzed using the method of computed fluid dynamics (CFD).

Methods—Twenty mathematical models of MCA vessels with aneurysms were created by 3-dimensional computed tomographic angiography. CFD calculations were performed by using our original finite-element solver with the assumption of Newtonian fluid property for blood and the rigid wall property for the vessel and the aneurysm.

Results—The maximum WSS in the calculated region tended to occur near the neck of the aneurysm, not in its tip or bleb. The magnitude of the maximum WSS was 14.39 ± 6.21 N/m^2, which was 4-times higher than the average WSS in the vessel region (3.64 ± 1.25 N/m^2). The average WSS of the aneurysm region (1.64 ± 1.16 N/m^2) was significantly lower than that of the vessel region ($P<0.05$). The WSSs at the tip of ruptured aneurysms were markedly low.

Conclusions—These results suggest that in contrast to the pathogenic effect of a high WSS in the initiating phase, a low WSS may facilitate the growing phase and may trigger the rupture of a cerebral aneurysm by causing degenerative changes in the aneurysm wall. The WSS of the aneurysm region may be of some help for the prediction of rupture. **(*Stroke*. 2004;35:2500-2505.)**

Key Words: aneurysm ■ biomechanics ■ hemodynamics ■ shear strength

Unruptured cerebral aneurysms are diagnosed with greater frequency since the development of increasingly accurate noninvasive cerebrovascular imaging techniques. Among 400 adult volunteers (39 to 71 years old; mean age, 55 years) who underwent clinical and radiological evaluations, Nakagawa et al reported the incidence of unruptured intracranial aneurysms to be as high as 6.5%.[1] Because the rupture of aneurysms results in subarachnoid hemorrhage, which has a dismal prognosis,[2,3] it is desirable to be able to determine whether a particular aneurysm has a high risk of rupture so that it can be treated before bleeding occurs. Aneurysms of a larger size (>10 mm) and/or a higher aspect ratio (>1.6) have a high risk of bleeding.[4–6] However, the majority of the unruptured aneurysms do not meet these criteria,[5] and it is difficult to predict the likelihood of their rupture.

Hemodynamic stresses are considered to have profound effects on the development of cerebral aneurysms.[7,8] One of these, the wall shear stress (WSS), acts directly on the vascular endothelium as a biological stimulator that modulates the cellular function of the endothelium.[9,10] Thus, the focus of the study presented here was aneurysm WSS. The close relationship between high WSS and the initiation of cerebral aneurysm formation has already been demonstrated in animal experiments.[11] The WSS may also play an important role in the growth and rupture of cerebral aneurysms.

The measurement of WSS in vivo is becoming feasible; however, it remains very difficult, especially in small and tortuous intracranial arteries.[12,13] With recent advances in computer technology, the magnitude and distribution of WSSs in complex arterial models have been observed with the aid of the computational fluid dynamics (CFD) technique, which is also a useful clinical tool for planning endovascular treatment.[14,15] The use of this technique has been limited to just a few cases; therefore, a statistical analysis of the results has not been possible. Here, we present the results of a

Received May 4, 2004; final revision received July 2, 2004; accepted August 10, 2004.

From the Department of Neurosurgery (M.S., A.M., T.K.), Faculty of Medicine, and the Institute of Industrial Science (M.S., M.O., R.T.), University of Tokyo, Japan; the Department of Neurosurgery (K.T.), Faculty of Medicine, Teikyo University, Japan; and the Departments of Neurosurgery (M.H.) and Radiology (K.K.), Faculty of Medicine, Fujita Health University, Japan.

Correspondence to Dr Masaaki Shojima, Department of Neurosurgery, Faculty of Medicine, University of Tokyo, Japan. 7-3-1, Hongo, Bunkyo-ku, Tokyo, Japan 113-0033. E-mail mshoji-tky@umin.ac.jp

Stroke is available at http://www.strokeaha.org

DOI: 10.1161/01.STR.0000144648.89172.of

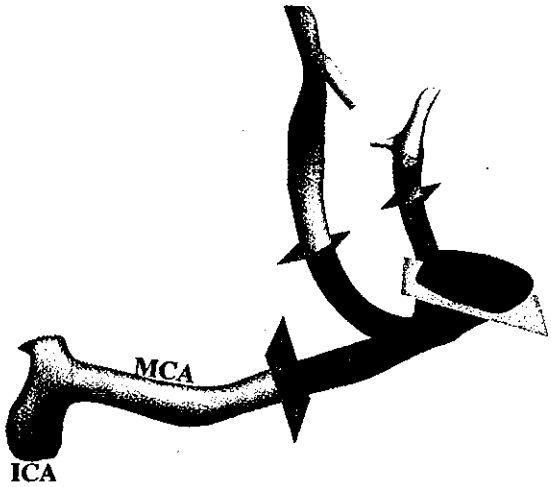

Figure 1. Extracted vessel image from 3-dimensional (3-D) computed tomographic angiography (after smoothing). The original model is trimmed out by the blue plane. The region to be analyzed (red) is divided into the aneurysm and the surrounding vessel by the yellow intersecting plane. ICA indicates internal carotid artery; MCA, middle cerebral artery.

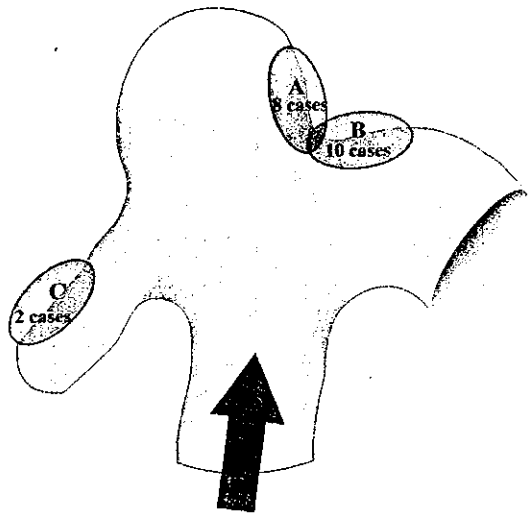

Figure 2. The sites where maximum wall shear stress (WSS) occurred in 20 cases. Eight occurred at the neck of the aneurysm (A), 10 at the origin of the branch artery in contiguity with the aneurysmal neck (B), and 2 in the branch vessel distant from the aneurysm (C).

statistical analysis of the magnitude of WSSs in and around saccular cerebral aneurysms.

Materials and Methods

Data Source

All medical data were acquired for diagnostic purposes, and consent for their use in this study was obtained from the patients or their closest relatives.

From January 2001 to December 2002, there were 42 middle cerebral artery (MCA) aneurysms that were diagnosed with 3-dimensional (3-D) computed tomographic (CT) angiography in 40 patients. Among them, 20 aneurysms of 19 patients had an adequate image quality for CFD calculation and were analyzed in this study. Patient population consisted of 7 men and 12 women, with a mean age of 61.5 years (range, 51 to 75 years). Three aneurysms were ruptured, and one of them was accompanied with an unruptured aneurysm. The other 16 aneurysms were detected before rupture by the screening examinations. All the aneurysm studied here were saccular aneurysms originating at the first major bifurcation of MCA.

Modeling of the Aneurysms

Three-dimensional CT angiography data with a voxel size of 0.21 mm×0.21 mm×0.50 mm were obtained with the aid of a multislice CT system,[16] the Aquilion multi 16 (Toshiba). The 16 central rows of 0.5-mm detector elements that were used had the following parameters: 0.75-second rotation, a scanning pitch of 0.69, 135 kV, and 260 mA. A total of 80 mL nonionic contrast medium (300 mg/mL) was injected at a rate of 3 mL/s via the median cubital vein. Digital images were transferred to a Unix workstation and vessel surfaces were constructed with the Fly-through mode of Alatoview (Toshiba). The fine irregularities of the original models resulting from partial volume effects or slice gaps were refined without changing the comprehensive geometry using our original smoothing software based on the algorithm of Garland mesh simplification[17] and Taubin mesh smoothing.[18] The aneurysm and the 20 mm of vessel surrounding it were trimmed out for the analysis. When possible, an intersecting plane dividing the aneurysm volume from that of the parent artery was made to allow a comparison of the WSS of the aneurysm and the vessel (Figure 1). Computational meshes were generated for these models with ≈60 000 hexahedral elements.

Numerical Simulation

CFD simulations were performed using our original finite-element solver under the governing equations of mass conservation and Navie–Stokes.[19–21] The boundary conditions were applied as follows. Blood was assumed to be an incompressible isothermal Newtonian fluid[22] with a specific gravity of 1000 kg/m^3 and a viscosity of 4.0×10^{-3} N/m^2 per second. The viscoelastic properties of the vessel wall were neglected and a rigid wall with no-slip condition was applied.[15] For the inlet condition, a pulsatile flow with a Womersley velocity profile was simulated,[23] with the typical MCA velocity obtained by transcranial Doppler scanning (mean velocity, 0.6 m/s; maximum velocity, 0.81 m/s; heart rate, 80 bpm). This inlet velocity condition was applied to all aneurysms (mean Reynolds number, 413; mean Womersley number, 3.99). A traction-free boundary condition[24] was applied to the outlets. The width of the time step for calculation was set at 0.0001 seconds.

To confirm numerical stability, the calculation was performed for 5 cardiac cycles and the result at the fifth cardiac cycle was used for

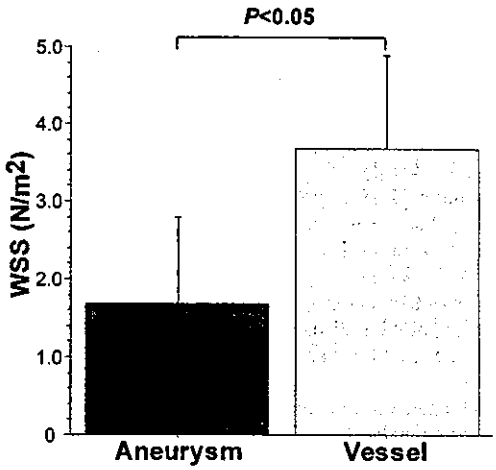

Figure 3. Comparison of WSSs between the aneurysm and vessel in 17 cases. The WSS of the aneurysm (red) is significantly lower than that of the vessel (yellow). Error bars indicate the standard deviation.

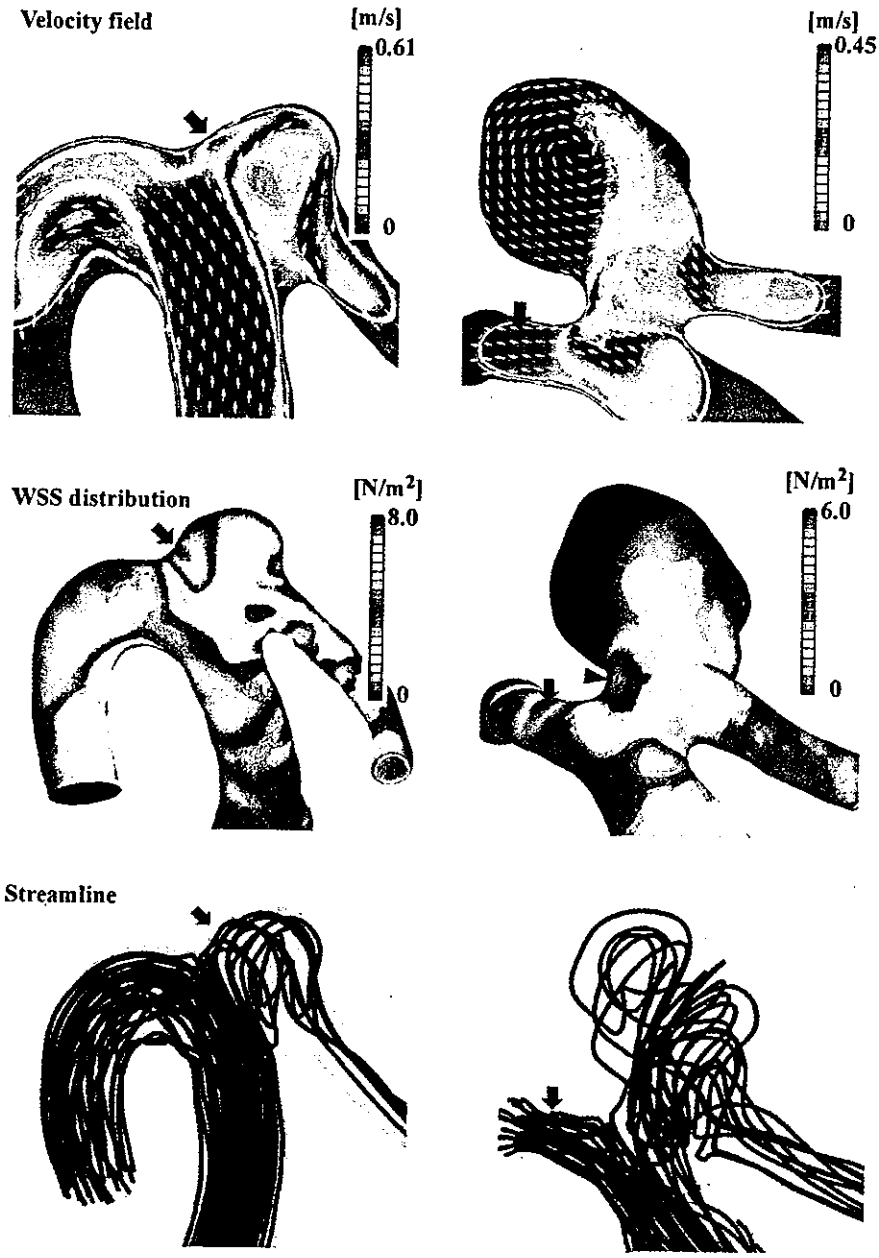

Figure 4. Visualization of the hemodynamics of 2 representative unruptured aneurysms (case 1, left; case 2, right). Arrows show the sites of maximum WSS. Top figures show velocity field in cross-sectional plane. Vectors show the direction of flow, and the magnitude of velocity is shown in colored contour. In case 1, interruption of flow at the bifurcation created a high-velocity field near the wall and caused a maximum WSS at the neck of the aneurysm. The intra-aneurysmal flow velocity was not decreased particularly in case 1. In contrast, in case 2, it was extremely low with a prominent recirculating zone in most parts of the aneurysm. Middle figures show WSS distribution in 3-D geometry. The maximum WSS occurred at the neck of the aneurysm in case 1. In case 2, a moderately high WSS occurred near the neck (arrow head), but the maximum WSS occurred at a site distant from the aneurysm where velocity increased as a result of reduction of the flow path. Bottom figures show the streamline, which shows the flow structure around the aneurysms. The lower part of the aneurysm in case 2 had flow structure similar to that in case 1. However, in case 2, the upper part had a stagnant disturbed flow structure, which led to a markedly low WSS.

the analysis. The calculation time for one aneurysm was ≈48 hours. WSS distributions were calculated from the 3-D velocity field data.[21]

Statistical Analysis

The maximum WSS region and its value were recorded for all aneurysms. When it was possible to divide the aneurysm from the parent artery with an intersecting plane, we calculated the spatially averaged WSS for each region at the peak systole. The WSS of the aneurysm was then compared with that of the vessel (paired Student *t* test). A nonpaired Student *t* test was applied to a comparison of the WSS of the ruptured aneurysms with that of the unruptured aneurysms.

For each aneurysm, the diameter of the inlet of the aneurysm and the maximum height of the aneurysmal sac from the inlet plane were measured from the 3-D model, and the aspect ratio was determined by dividing the latter by the former. Pearson correlation coefficients were calculated among the aspect ratio, the WSS of the aneurysm region, and the volumetric flow into the aneurysm. Statistical significance was taken as $P<0.05$.

Results

Magnitude and Distribution of WSSs

The sites where the maximum WSS occurred in the calculated region could be divided into 3 groups (Figure 2). In 10 aneurysms, the maximum WSS appeared at the origin of the branch artery in contiguity with the aneurysmal neck. In 8 aneurysms, the sites were at the neck of the aneurysm, and in the remaining 2 the maximum WSS occurred in the branch artery distant from the aneurysm. Whereas moderately high WSSs appeared at the body of the aneurysm in some cases, the WSSs at the tip or the bleb of the aneurysm were markedly low in all aneurysms. The peak WSS value averaged over the 20 cases was 14.39 ± 6.21 N/m^2 (mean±SD; 1 N/m^2=0.0075 mm Hg or 10 dyne/cm^2), which was 4-times higher than the spatially averaged WSS of the vessel region at the peak systole (3.64 ± 1.25 N/m^2).

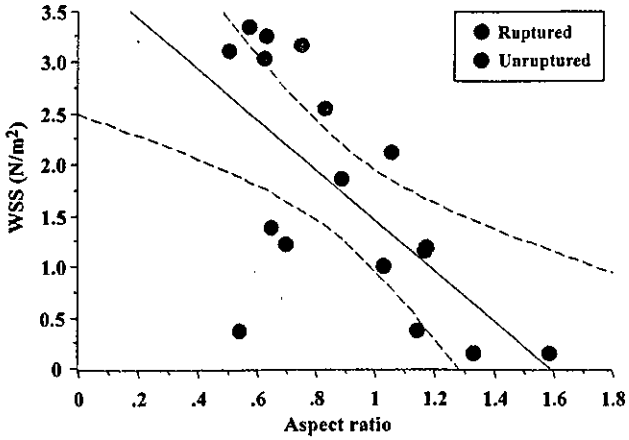

Figure 5. Bivariate scattergram with regression between the aspect ratio and the WSS of the aneurysm. A significant negative correlation can be observed ($r=-0.67$). Ruptured cases are shown as red, and unruptured cases are shown as blue. Dotted lines indicate 95% confidence bands.

Intersecting planes dividing the aneurysm from the parent artery were created successfully for all but 3 small unruptured aneurysms. For these 17 cases, the WSS of the vessel region (spatially averaged at the peak systole) was 3.64 ± 1.25 N/m^2. In contrast, the WSS of the aneurysm region (spatially averaged at the peak systole) was 1.64 ± 1.16 N/m^2, which is significantly lower than that of the vessel ($P<0.05$; Figure 3).

Flow Structure in the Aneurysms

The shape of the aneurysm had a profound impact on the flow structure within it. In case 1 (Figure 4, left), a small aneurysm with a smooth contour and a low aspect ratio of 0.56, the intra-aneurysmal flow velocity did not decrease particularly. The averaged WSS of the aneurysm region at the peak systole was 3.35 N/m^2, one of the highest among our cases. However, in case 2, which had a large aneurysm with an aspect ratio of 1.58 (Figure 4, right), the intra-aneurysmal flow velocity was markedly low and the flow field showed a conspicuous recirculating zone. In this case, the spatially averaged WSS of the aneurysm region was markedly low (0.14 N/m^2) even at the peak systole because of this large area of the flow stasis.

The aspect ratio of the aneurysm had a significant negative correlation ($r=-0.67$, $P<0.05$; Figure 5) with the WSS of the aneurysm region (spatially averaged at the peak systole). A mild positive correlation was observed between the spatially averaged WSS of the aneurysm region and the volumetric flow into the aneurysm ($r=0.50$, $P=0.06$). The correlation between the volumetric flow into the aneurysm and the aspect ratio of the aneurysm was weak ($r=0.36$, $P=0.06$).

Ruptured Versus Unruptured Aneurysms

The mean size (diameter) and the aspect ratio of the aneurysms were 3.36 mm and 0.73, respectively, for the ruptured cases (n=3) and 4.31 mm and 0.92, respectively, for the unruptured cases (n=17). The difference between the respective figure for the ruptured and unruptured cases was not statistically significant.

When the spatially averaged WSS of aneurysm region at the peak systole was compared between ruptured and unruptured cases, it was found to be significantly higher for ruptured cases (2.92 N/m^2 versus 1.48 N/m^2, $P<0.05$).

In all ruptured cases, high and low WSS were mixed in the small aneurysm area (Figure 6). The blood of parent artery flowed into the aneurysm more directly in the ruptured cases and high WSSs appeared at the body or the neck of aneurysm.

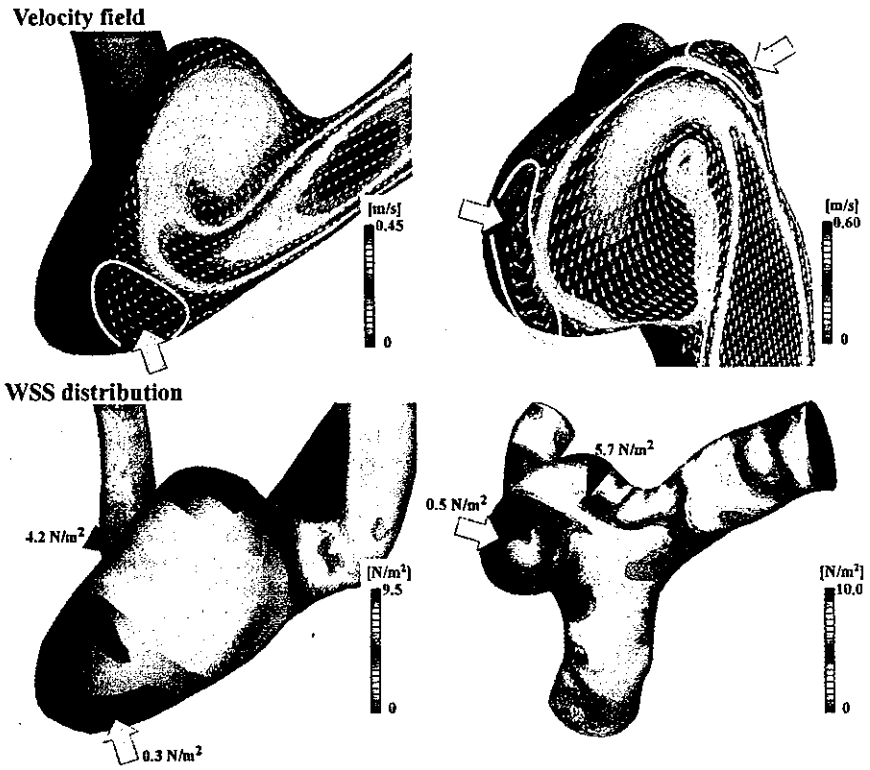

Figure 6. Velocity field and WSS distribution of 2 ruptured aneurysms. The velocity field in cross-sectional plane (upper) and the WSS distribution in 3-D geometry (lower) are shown in the same way as Figure 4. Black arrowheads indicate the site of moderately elevated WSSs in the aneurysm region. Yellow arrows and lines show the site of a markedly low WSS area and the flow stasis with recirculating zones at the tip of the aneurysm, respectively. The numbers near the arrows indicate the magnitude of WSSs at the sites.

This resulted in a higher averaged WSS of the aneurysm region in ruptured cases. However, at the tip, the stasis of the blood with recirculating zones was observed. This caused markedly low WSS at the tip (<0.5 N/m^2). These findings make fine contrast to the flow structure of the unruptured aneurysm, shown in the left side of Figure 4, which also had a high averaged WSS of the aneurysm region. The intra-aneurysmal velocity was not delayed, particularly near the wall. The WSS at the tip of this unruptured aneurysm was not decreased severely (1.7 N/m^2).

Discussion

This study demonstrates clearly that the magnitude of the WSS of the aneurysm region is significantly lower than that of the vessel region. The present study also disclosed that the WSS of the aneurysm region has a significant and inverse correlation with the aspect ratio of aneurysm, which has some connection to the rupture.[4,5]

WSS is a flow-induced stress that can be described as the frictional force of viscous blood.[10] The 3-D geometry and the 3-D velocity field of vessels are indispensable to the establishment of spatial distribution of WSS and the flow structure. In vivo measurements of the 3-D velocity field and WSS have become possible with the development of phase contrast magnetic resonance velocimetry for large and simple arteries like the aorta[25] or the carotid bifurcation.[13] However, in small and tortuous vessels like the intracranial arteries, the currently available techniques, like phase contrast magnetic resonance velocimetry, cannot be applied in calculating the spatial distribution of the WSS. To investigate the flow dynamics in cerebral arteries, simulation in vitro or by computer is necessary. The major difference between in vitro fluid experiments and CFD simulations may be the fact that the quality of computational mesh generation has some effect on the results of computer simulations. However, the reliability of computer simulations with proper mesh generation has been established.[24] Comparisons between our results and those of in vitro experiments are ongoing in our laboratory.[20]

Recent studies have indicated the involvement of WSS in the formation of saccular cerebral aneurysms.[11] A prolonged high WSS fragments the internal elastic lamina of vessels[26] and gives rise to the initial change involved in the formation of a cerebral aneurysm. Our results have established that the magnitude of the WSS of well-developed aneurysms is very low, in accordance with the previous hypothesis that the strength of the WSS of the aneurysm region is not sufficient to mechanically tear the wall of the aneurysm.[7] The WSS is converted to biological signals via mechanoreceptors on endothelial cells, and it modulates gene expressions and the cellular functions of the vessel wall.[9,10] It is assumed that a WSS of ≈2.0 N/m^2 is suitable for maintaining the structure of arterial vessels and a WSS lower than 1.5 N/m^2 will degenerate endothelial cells via the apoptotic cell cycle.[10] The WSS of the aneurysm region was barely 1.64 N/m^2 even in the peak systole and seems to be too low to maintain the regular cellar functions of endothelial cells. This excessively low WSS may be one of the main factors underlying the degeneration, indicating the structural fragility of the aneurysmal wall. Although a high WSS plays an essential role in the initiation of cerebral aneurysms,[11] a low WSS might be a major factor for its growth.

Our 3 ruptured aneurysms had higher averaged WSS of aneurysm region than unruptured aneurysms and they had markedly low WSS in their tip or bleb with high WSS in the body or fundus of aneurysm. We speculate that this low WSS at the tip or the bleb might be responsible for the fragile change of the aneurysm and led to the rupture. Endothelial cells react differently to the high and low WSS.[10] The proximity of high and low WSS in a small aneurysm region might enhance the degenerative change of the aneurysm wall.

Until now, there has been no study to our knowledge that demonstrated the changes of the size and the shape of the aneurysm immediately before and after the rupture. These changes might have affected our results. The current and previous[4,5] results of ruptured aneurysms might not characterize the aneurysm with high risk of rupture, but may only document the feature of the aneurysm after rupture. The application of these results to the clinical materials will prove the validity.

Conclusions

The results of this study suggest that the CFD technique has the potential to be a useful clinical tool for the prediction of the initiation, growth, and rupture of cerebral aneurysms.

References

1. Nakagawa T, Hashi K. The incidence and treatment of asymptomatic, unruptured cerebral aneurysms. *J Neurosurg*. 1994;80:217–223.
2. Hop JW, Rinkel GJ, Algra A, van Gijn J. Case-fatality rates and functional outcome after subarachnoid hemorrhage: a systematic review. *Stroke*. 1997;28:660–664.
3. Takagi K, Tamura A, Nakagomi T, Nakayama H, Gotoh O, Kawai K, Taneda M, Yasui N, Hadeishi H, Sano K. How should a subarachnoid hemorrhage grading scale be determined? A combinatorial approach based solely on the Glasgow Coma Scale. *J Neurosurg*. 1999;90:680–687.
4. Ujiie H, Tachibana H, Hiramatsu O, Hazel AL, Matsumoto T, Ogasawara Y, Nakajima H, Hori T, Takakura K, Kajiya F. Effects of size and shape (aspect ratio) on the hemodynamics of saccular aneurysms: a possible index for surgical treatment of intracranial aneurysms. *Neurosurgery*. 1999;45:119–129; discussion 129–30.
5. Weir B, Amidei C, Kongable G, Findlay JM, Kassell NF, Kelly J, Dai L, Karrison TG. The aspect ratio (dome/neck) of ruptured and unruptured aneurysms. *J Neurosurg*. 2003;99:447–451.
6. International Study of Unruptured Intracranial Aneurysms Investigators. Unruptured intracranial aneurysms–risk of rupture and risks of surgical intervention. International Study of Unruptured Intracranial Aneurysms Investigators. *N Engl J Med*. 1998;339:1725–1733.
7. Steiger HJ. Pathophysiology of development and rupture of cerebral aneurysms. *Acta Neurochir Suppl (Wien)*. 1990;48:1–57.
8. Stehbens WE. Etiology of intracranial berry aneurysms. *J Neurosurg*. 1989;70:823–831.
9. Gibbons GH, Dzau VJ. The emerging concept of vascular remodeling. *N Engl J Med*. 1994;330:1431–1438.
10. Malek AM, Alper SL, Izumo S. Hemodynamic shear stress and its role in atherosclerosis. *JAMA*. 1999;282:2035–2042.
11. Kondo S, Hashimoto N, Kikuchi H, Hazama F, Nagata I, Kataoka H. Cerebral aneurysms arising at nonbranching sites. An experimental study. *Stroke*. 1997;28:398–403; discussion 403–404.
12. Milner JS, Moore JA, Rutt BK, Steinman DA. Hemodynamics of human carotid artery bifurcations: computational studies with models reconstructed from magnetic resonance imaging of normal subjects. *J Vasc Surg*. 1998;28:143–156.
13. Papathanasopoulou P, Zhao S, Kohler U, Robertson MB, Long Q, Hoskins P, Xu XY, Marshall I. MRI measurement of time-resolved wall shear stress vectors in a carotid bifurcation model, and com-

parison with CFD predictions. *J Magn Reson Imaging*. 2003;17: 153–162.
14. Steinman DA, Milner JS, Norley CJ, Lownie SP, Holdsworth DW. Image-based computational simulation of flow dynamics in a giant intracranial aneurysm. *AJNR Am J Neuroradiol*. 2003;24:559–566.
15. Jou LD, Quick CM, Young WL, Lawton MT, Higashida R, Martin A, Saloner D. Computational approach to quantifying hemodynamic forces in giant cerebral aneurysms. *AJNR Am J Neuroradiol*. 2003;24:1804–1810.
16. Katada K, Fujii N, Banno T, Nakane M. Usefulness of isotropic volumetric data in neuroradiological diagnosis. In: Reiser MF, Takahashi M, Modic M, Becker CR, eds. *Multislice CT*, 2nd revised ed. Berlin, Heidelberg, New York: Springer-Verlag; 2004:45–52.
17. Garland M, Heckbert PS. Surface simplification using quadric error metrics. In: *SIGGRAPH 97*. Los Angeles, California: ACM Press/ Addison-Wesley Publishing Co; 1997:209–216.
18. Taubin G. Curve and surface smoothing without shrinkage. *The Fifth International Conference on Computer Vision (ICCV 95)*. Cambridge, Massachusetts: IEEE Computer Society; 1995:852–857.
19. Ooshima M, Takagi K, Hayakawa M. [Image-based simulation of cerebral aneurysms]. *Igaku Butsuri*. 2003;23:209–214. In Japanese.
20. Oshima M, Kobayashi T, Takagi K. Biosimulation and visualization: effect of cerebrovascular geometry on hemodynamics. *Ann N Y Acad Sci*. 2002;972:337–344.
21. Oshima M, Torii R, Kobayashi N, Taniguchi N, Takagi K. Finite element simulation of blood flow in the cerebral artery. *Comput Methods Appl Mech Eng*. 2001;191:661–671.
22. Brooks DE, Goodwin JW, Seaman GV. Interactions among erythrocytes under shear. *J Appl Physiol*. 1970;28:172–177.
23. Taylor CA, Hughes TJR, Zarins CK. Finite element modeling of blood flow in arteries. *Comput Methods Appl Mech Eng*. 1998;158:155–196.
24. Zienkiewicz OC, Taylor RL. *The Finite Element Method*, 4th ed. London, UK: McGraw-Hill; 1994.
25. Wood NB, Weston SJ, Kilner PJ, Gosman AD, Firmin DN. Combined MR imaging and CFD simulation of flow in the human descending aorta. *J Magn Reson Imaging*. 2001;13:699–713.
26. Masuda H, Zhuang YJ, Singh TM, Kawamura K, Murakami M, Zarins CK, Glagov S. Adaptive remodeling of internal elastic lamina and endothelial lining during flow-induced arterial enlargement. *Arterioscler Thromb Vasc Biol*. 1999;19:2298–2307.